analytical chemistry

Article

Cite This: Anal. Chem. 2019, 91, 15267−15274

pubs.acs.org/ac

# N-Doped Carbon As Peroxidase-Like Nanozymes for Total Antioxidant Capacity Assay

Zhangping Lou,[†] Sheng Zhao,[†] Quan Wang,[†] and Hui Wei*[,†,‡,§]

[†]Department of Biomedical Engineering, College of Engineering and Applied Sciences, Nanjing National Laboratory of Microstructures, Jiangsu Key Laboratory of Artificial Functional Materials, Chemistry and Biomedicine Innovation Center (ChemBIC), Nanjing University, Nanjing, Jiangsu 210093, China

[‡]State Key Laboratory of Analytical Chemistry for Life Science and State Key Laboratory of Coordination Chemistry, School of Chemistry and Chemical Engineering, Nanjing University, Nanjing, Jiangsu 210023, China

[§]Key Laboratory of Analytical Chemistry for Biology and Medicine (Wuhan University), Ministry of Education, Wuhan University, Wuhan, Hubei 430072, China

Supporting Information

**ABSTRACT:** N-doping strategy has been explored to enhance the activity of carbon nanozymes because the reconstructed electronic structures in N-doped carbon nanozymes are advantageous for the catalytic process. However, carbon nanozymes with high N content are still difficult to obtain due to the instability of N element under high calcination temperatures. To address this challenge, here we proposed a new N-doping strategy to fabricate highly active and specific peroxidase-like carbon nanozymes by using a high N-containing polymer (i.e., polyethylenimine (PEI)) as the N source and a natural clay mineral (i.e., montmorillonite (MMT)) as a template, respectively. We showed that the assembly of MMT with PEI protected N loss under high calcination temperatures and thus retained more catalytically active N sites. The mechanism study showed that the hydroxyl radical could be the key intermediate involved in the peroxidase-like catalysis. We then used the optimized carbon nanozyme with high and specific peroxidase-like activity (i.e., $CP_{600-6}$) to detect $H_2O_2$, glucose, and ascorbic acid. Moreover, we successfully determined the total antioxidant capacity (TAC) in real samples including four commercial beverages, fresh orange juice, and three kinds of vitamin C tablets. The current study not only provides a new strategy for fabricating peroxidase-like nanozymes but also develops a facile TAC assay for future use in evaluation of antioxidant food quality and oxidative stress in healthcare.

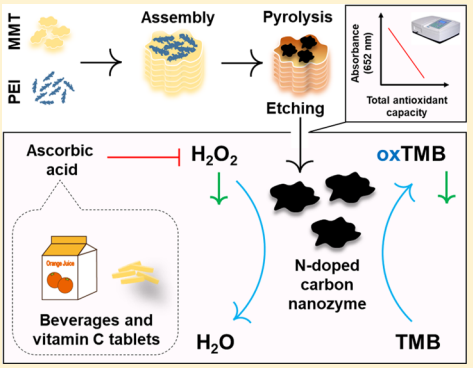


## INTRODUCTION

Nanozymes have received considerable attention recently because of their superior properties compared with both natural enzymes and conventional enzyme mimics.[1−11] Till now, various enzyme-like nanozymes have been developed, such as peroxidase mimics, oxidase mimics, catalase mimics, superoxide dismutase mimics, and hydratase mimics.[12−23] Among them, peroxidase-like nanozymes are of particular interest due to their broad applications in analytical detection as well as disease diagnosis and therapy.[12,19,24−26] For example, peroxidase-like nanozymes have been constructed to detect bioactive small molecules (such as $H_2O_2$, glucose, and ascorbic acid (AA, vitamin C)), metal ions (such as $Ag^+$, $Hg^{2+}$, and $Ce^{3+}$), nucleic acids, proteins, and even viruses.[24,26−34] Despite of this progress, to the best of our knowledge, no studies have been devoted to the detection of total antioxidant capacity (TAC) by using peroxidase-like nanozymes. TAC is a critical parameter to access the food quality and the oxidative stress in healthcare. To fill this gap, herein we developed an assay to detect the TAC by using N-doped carbon nanozymes with peroxidase-like activities.

Peroxidases have been mimicked by using lots of nanomaterials, including metals, metal oxides, metal−organic frameworks, carbon, etc.[1,9,19,35−38] Among them, carbon nanomaterial-based peroxidase mimics are attractive due to their high stability, low cost, and good biocompatibility. However, the peroxidase-like activities of developed carbon nanozymes were moderate.[9] Therefore, several strategies including heteroatom doping have been proposed to enhance the catalytic activities of carbon nanozymes by others and us.[39−43] For instance, we have demonstrated that the N-doping selectively enhanced the peroxidase-like activities of reduced graphene oxide and mesoporous carbon.[40] For these developed strategies, the amount of N could be doped was limited. Therefore, new strategies are still needed to develop highly active peroxidase-like carbon nanozymes with high N-doping.

In this work, we proposed a template method to synthesize high N-containing carbon nanozymes by using a negatively

Received: September 23, 2019
Accepted: November 6, 2019
Published: November 6, 2019






DOI: 10.1021/acs.analchem.9b04333
Anal. Chem. 2019, 91, 15267−15274

**Scheme 1. Schematic Illustration of the Synthesis Process of N-Doped Carbon Sheets Based on the Strong Electrostatic Attraction between MMT and PEI**

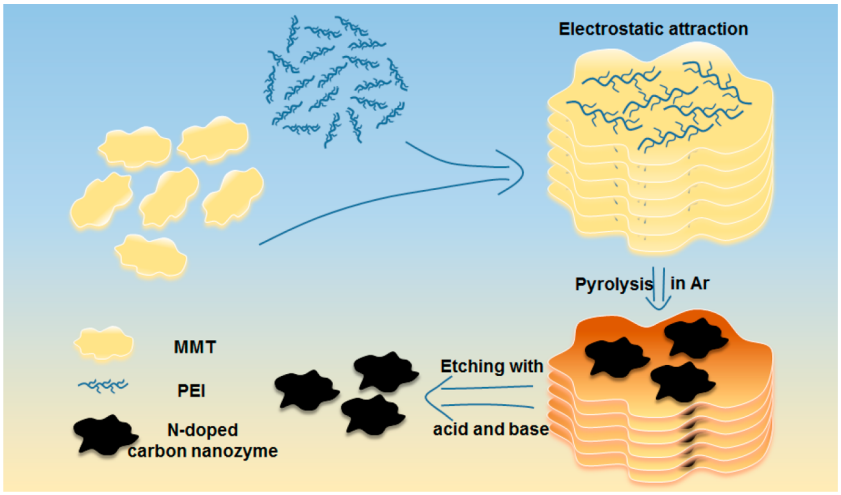


charged natural clay mineral (i.e., montmorillonite, MMT) as a hard template and a positively charged polyethylenimine (PEI) with high nitrogen−carbon ratio as carbon and nitrogen source, respectively (Scheme 1 and Figure S1). We showed that the peroxidase-like activity of the N-doped carbon nanozymes could be modulated by the molecular weight of PEI and the pyrolysis temperature. After having elucidated the catalytic mechanism, the carbon nanozyme with the highest peroxidase-like activity was used to develop assays for hydrogen peroxide, glucose, and AA. Moreover, a TAC assay was further developed by using the carbon nanozyme and the TAC in drinks and medical tablets were successfully determined (the TAC was expressed as AA equivalent antioxidant capacity).

## EXPERIMENTAL SECTION

**Chemicals and Materials.** Polyethylenimine (PEI), 3,3′,5,5′-tetramethylbenzidine (TMB), 2,2′-azino-bis(3-ethylbenzothiazoline-6-sulfonic acid) (ABTS), *o*-phenylenediamine (OPD), maltose, dihydroethidium (HE), and glucose oxidase (GOx) were purchased from Aladdin Chemical Reagent Co., Ltd. Montmorillonite (Na-MMT, PGW) was purchased from Nanocor company. Glucose and sucrose were purchased from Nanjing Chemical Reagent Co., Ltd. Fructose was purchased from Shandong Xiya Reagent Co., Ltd. Galactose was purchased from Huixing Biochemical Reagents Co., Ltd. Ascorbic acid (AA) and hydrogen peroxide ($H_2O_2$) were purchased from Sinopharm Chemical Reagent Co., Ltd. All chemical reagents were used as received without further purification. All aqueous solutions used in the experiments were prepared with deionized water (18.2 MΩ·cm, Millipore).

**Instrumentation.** Transmission electron microscopy (TEM) images were collected on a JEM-2100 electron microscope (JEOL, Japan) at an acceleration voltage of 200 kV. Powder X-ray diffraction (XRD) patterns were collected on a Thermo Fisher Scientific XTRA diffractometer by using Cu K$\alpha$ radiation. X-ray photoelectron spectroscopy (XPS) was obtained using a PHI 5000 VersaProbe (Ulvac-Phi, Japan). UV−visible absorption spectra were recorded using a TU-1900 spectrophotometer (Beijing Purkinje General Instrument Co. Ltd., China). Zeta potential distributions were measured on a Zetasizer Nano (Malvern, U.K.). Pyrolysis tests were carried out on a Pyris 1 DSC thermogravimetric (TG) analyzer under the $N_2$ atmosphere with a heating rate of 10 °C·min$^{-1}$. Raman spectra were recorded using a Renishaw inVia Raman spectrometer, equipped with a Leica DMI300B inverted microscope and a Peltier-cooled charge-coupled device (CCD) detector. Infrared spectra were recorded using an NEXUS870 Fourier transform infrared spectrometer (Nicloet, U.S.A.). The absorption in testing $H_2O_2$, glucose, and AA was recorded using a SpectraMax M2e microplate reader (Molecular Devices, U.S.A.). Fluorescence spectra were recorded using a F-4600 fluorescent spectrometer (Hitachi, Japan). The EPR signals of the $^{\bullet}$OH free radicals captured by DMPO (DMPO−OH) were recorded using an EMX-10/12 spectrometer (Bruker, Germany).

**Synthesis of N-Doped Carbon Nanozymes.** As shown in Scheme 1, the N-doped carbon nanozymes were synthesized as follows.[41,42] First, both MMT and PEI aqueous solutions with 2 wt % concentration were prepared and stirred vigorously for 24 h. For the MMT solution, it was left to stay overnight, the supernatant was then collected as the MMT nanosheet solution for further use. The pH of PEI solution was adjusted to 7.0 with a 60 wt % acetic acid solution. Then, the MMT nanosheet solution was mixed with PEI solution at a ratio of 5:1 v/v under vigorous stirring. The mixed solution was lyophilized to obtain the assemblies powder (MP). After that, the MP was calcinated in a tube furnace at the setting temperatures for 3 h with a temperature ramp rate of 5 °C·min$^{-1}$. Finally, the N-doped carbon nanozymes (CP) were obtained by etching the MMT in calcinated products using both 10 M NaOH and HCl alternately.

**Enzyme Mimicking Activities of N-Doped Carbon Nanozymes.** The peroxidase-like activity was measured using TMB, ABTS, or OPD as a substrate. Typically, acetic acid-sodium acetate buffer (pH 4.0, 0.2 M) containing 5 mM $H_2O_2$, 500 $\mu$M substrate, and 10 $\mu$g/mL CP was mixed thoroughly. After mixing, the reaction solution was immediately used for UV−visible spectroscopic measurements.

The oxidase-like activity was measured by using the same protocol as the peroxidase mimics except without adding $H_2O_2$ solution.



DOI: 10.1021/acs.analchem.9b04333
*Anal. Chem.* 2019, 91, 15267−15274

The catalase-like activity was measured by monitoring the absorption of the mixture containing $H_2O_2$ and CP at 240 nm with the UV−visible spectrophotometer.

The SOD-like activity was measured by the HE method. Typically, PBS buffer (pH 7.4, 0.1 M) containing xanthine (0.6 mM), xanthine oxidase 0.05 U/L), and CP (5 μg/mL) was incubated for 10 min at 37 °C. Then HE (final concentration of 0.1 mg/L) was added and further incubated for 30 min. The fluorescence spectra were recorded ($\lambda_{ex}$ = 470 nm and $\lambda_{em}$ = 610 nm).

**Catalytic Mechanism for Peroxidase-Like Activity.** To understand the catalytic mechanism of the peroxidase-like nanozymes, the potential intermediates were captured and monitored. For $^{\bullet}OH$ radicals, PBS buffer (pH 6.0, 25 mM) containing 1 mM $H_2O_2$, 100 μg/mL CP, and 0.5 mM TA was incubated at 37 °C for 12 h, then the fluorescence spectra were recorded ($\lambda_{ex}$ = 315 nm and $\lambda_{em}$ = 435 nm). For $^{\bullet}O_2^-$ radicals, acetic acid-sodium acetate buffer (pH 4.0, 0.2 M) containing 10 mM $H_2O_2$, 100 μg/mL CP, and 100 μg/mL HE was incubated at 37 °C for 40 min, and then the fluorescence spectra were recorded ($\lambda_{ex}$ = 470 nm and $\lambda_{em}$ = 610 nm). For further verification, EPR was applied to probe the $^{\bullet}OH$ and $^{\bullet}O_2^-$ radicals. Acetic acid-sodium acetate buffer (pH 4.0, 0.2 M) containing 0.02 mM $H_2O_2$, 100 μg/mL CP, and 100 mM DMPO was incubated for 30 min and the mixture was transferred into a capillary tube for EPR measurements.

**Kinetics Study.** Steady-state kinetics assays were performed at 37 °C in a 1 mL cuvette with a path length of 0.2 cm. To determine the affinity between CP and TMB, acetic acid-sodium acetate buffer (pH 4.0, 0.2 M) containing $H_2O_2$ (50 mM), 10 μg/mL CP, and TMB (25 μM-800 μM) was mixed. After 1 min, the absorption at 652 nm was monitored immediately. Similarly, to determine the affinity between CP and $H_2O_2$, TMB with constant concentration (1 mM) and $H_2O_2$ with varying concentration of (2.5 mM to 80 mM) were used. The kinetics constants (i.e., $v_{max}$ and $K_m$) were calculated by fitting the reaction velocity values and the substrate concentrations to the Michaelis−Menten equation as follows:

$$v = \frac{v_{max}[S]}{K_m + [S]} \quad (1)$$

where $v$ is the initial reaction velocity, $v_{max}$ is maximal reaction velocity, [S] is the substrate concentration, and $K_m$ is the Michaelis constant.

**$H_2O_2$ Detection.** Acetic acid-sodium acetate buffer (pH 4.0, 0.2 M) containing $H_2O_2$ (0−10 mM), 10 μg/mL CP, and TMB (500 μM) was incubated for 2 min. Then 200 μL of the reaction solution was added into 96-well plate and the absorption at 652 nm was recorded in a microplate reader.

**Glucose Detection.** The detection was carried out as follows. First, tris-HCl buffer (pH 7.0) containing 1 mg/mL GOx and glucose with various concentrations (0−3 mM) was incubated at 37 °C for 30 min to produce $H_2O_2$. Then, another acetic acid-sodium acetate buffer (pH 4.0, 0.2 M) containing TMB and CP solutions was added. The final concentrations of TMB and CP were 500 μM and 10 μg/mL, respectively. The reaction solution was incubated for another 15 min at 37 °C. Finally, 200 μL of the reaction solution was added into 96-well plate and the absorption at 652 nm was recorded in a microplate reader.

To investigate the selectivity of the above assay for detection of glucose, fructose, lactose, and sucrose with a concentration of 5 mM and glucose with a concentration of 1 mM were determined.

**AA Detection.** Acetic acid-sodium acetate buffer (pH 5.0, 0.2 M) containing 0.1 M $H_2O_2$, 500 μM TMB, 10 μg/mL CP, and AA with various concentrations (0−1 mM) was incubated for 15 min at 37 °C. Then, 200 μL of the reaction solution was added into 96-well plate and the absorption at 652 nm was recorded in a microplate reader.

To investigate the selectivity of the above assay for detection of AA, metal ions ($Na^+$, $K^+$, $Ca^{2+}$, $Cu^{2+}$, and $Fe^{3+}$), amino acid (glycine, glutamic acid, arginine, lysine, proline, histidine, and cysteine), carbohydrates (glucose, maltose, fructose, lactose, and sucrose), glutathione, and BSA as interference were determined. The concentration of the above five metal ions, amino acids except cysteine and the five carbohydrates were 2 mM, which was 10 times the concentration of AA (0.2 mM). The concentrations of cysteine, glutathione, and BSA were 0.2 mM, 0.2 mM, 25 mg/mL, respectively.

**TAC Detection.** The same protocol for AA detection was applied to the TAC detection of four commercial beverages, fresh orange juice, and aqueous solutions of three vitamin C tablets. The concentrations of all of the above samples were adjusted to fit in the linear range of AA detection. The TAC of all of the samples was expressed as millimolar equivalent of AA/L.

## RESULTS AND DISCUSSION

**Synthesis and Characterization of N-Doped Carbon Nanozymes.** Two methods including evaporating and freeze-drying were used to prepare the PEI hybridized montmorillonite assemblies (MP, Figure S2). The MP prepared by the evaporating method possessed "brick-and-mortar" layered microstructures like natural nacre.[44] Interestingly, the MMT sheets were arrayed along the same orientation, which was not dependent on the PEI precursors (i.e., PEI with molecular weight of 600 vs 10000). This result indicated that PEI played the role of glue between MMT sheets (Figure S2a,c). While the MP prepared by the freeze-drying method exhibited the disordered structures with abundant micropores (Figure S2b,d). The peroxidase-like activities of the N-doped carbon nanozymes derived from the two MPs were compared. As shown in Figure S2e, the nanozymes via the freeze-drying method showed higher activities. Besides, compared with the evaporating method, the freeze-drying method was more controllable. Therefore, the freeze-drying method was chosen for synthesizing all the following samples. The MP samples were then calcinated at various temperatures (i.e., 400, 600, and 800 °C), and subsequently etched by base and acid alternately. For simplicity, the final N-doped carbon nanozymes using the freeze-drying method were named as $CP_{600-4}$, $CP_{600-6}$ and $CP_{600-8}$, and $CP_{10000-6}$, where CP referred to carbon-based peroxidase mimic; 600 and 10000 to PEI molecular weights; and the subscript numbers (i.e., 4, 6, and 8) to calcination temperatures.

The synthetic process was followed by measuring the XRD patterns of MPs, calcinated MPs, and CPs. As shown in Figure S3a, the diffraction peak at 7.2° of MMT shifted to 6.5° for $MP_{600}$ and 6.4° for $MP_{10000}$, respectively. The shift indicated that the insertion of PEI broadened the space between MMT sheets. Moreover, the larger shift for $MP_{10000}$ suggested that PEI with a higher molecular weight could broaden the space in a greater extent. After the calcination, the corresponding MMT peaks decreased. The more decrease was well correlated with



DOI: 10.1021/acs.analchem.9b04333
Anal. Chem. 2019, 91, 15267−15274

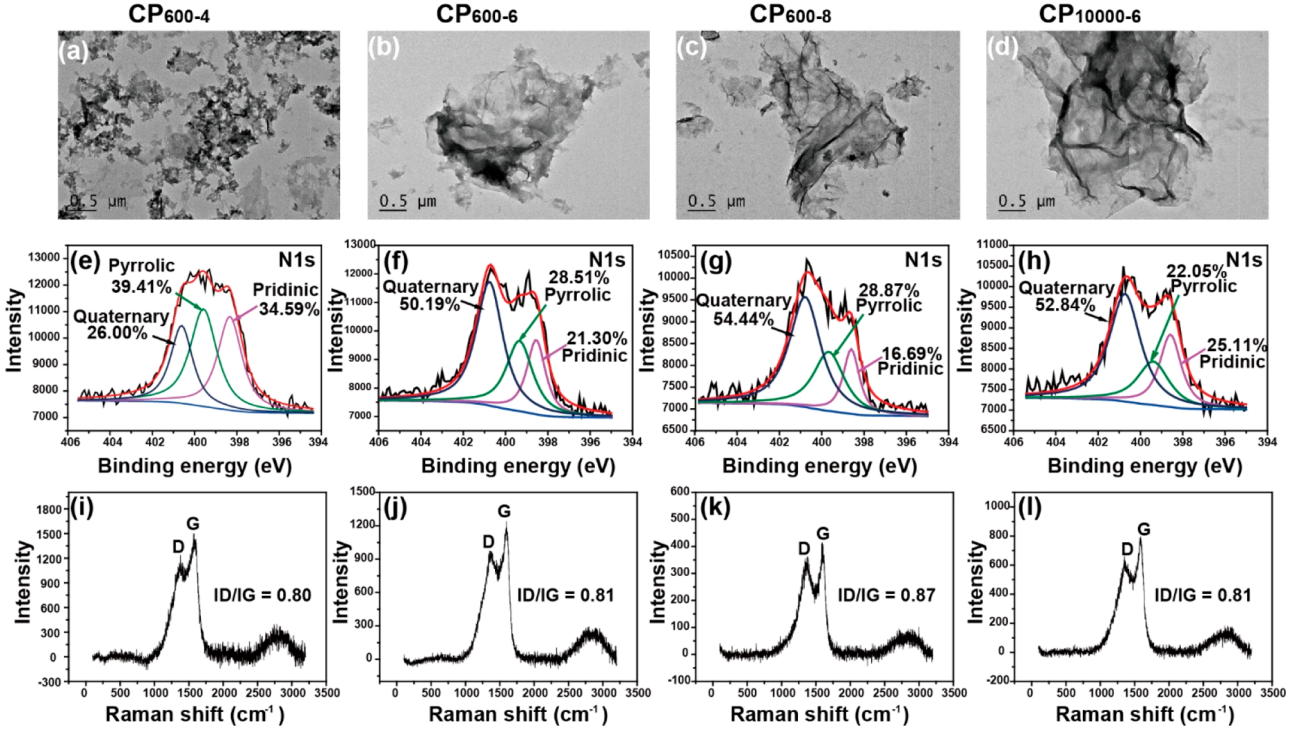


**Figure 1.** TEM images, N 1s core level XPS spectra, and Raman spectra of (a, e, and i) $CP_{600-4}$, (b, f, and j) $CP_{600-6}$, (c, g, and k) $CP_{600-8}$, and (d, h, and l) $CP_{10000-6}$.

the higher calcination temperature (Figure S3b). After treating with acid and base, no remaining MMT peak was found, indicating the successful etching of MMT. All four CPs exhibited broad peaks centered at about 25°, which were corresponding to a layer spacing of 0.356 nm and was consistent with N-doped carbon materials (Figure S3c).[45,46]

The formed CP nanozymes were then characterized by TEM imaging. As shown in Figure 1a–d, for all four CPs, no MMT sheets were observed. Moreover, $CP_{600-4}$ had irregular fragments while the other three showed similar stacked carbon sheets with several micrometers in size. The observed fragments indicated that 400 °C was not high enough to complete the carbonization process. To further understand the effect of calcination temperature, the pyrolysis characteristics of MP were investigated by TG analysis (Figure S4). The TG results demonstrated that as high as 600 °C was needed for completing calcination process, agreeing with the above TEM imaging results.

XPS analyses were carried out to determine the elemental compositions of the nanozymes and the configuration of the doped nitrogen. From XPS survey scan, C, O, and N were found in all the four CPs (Figure S5). Interestingly, the CPs also possessed high content of N (4.65–7.53%), which was higher than that of several N-doped carbon nanomaterials synthesized by hard template methods (Table S1).[47−50] Such a high N content could be attributed to PEI with high N/C ratio and the shielding effect of MMT. Note, no peaks of Si and Al from MMT could be seen in the XPS spectra, confirming the successful etching of MMT. The N configuration was then analyzed from the high resolution N 1s spectra (Figure 1e–h). Three N configurations (i.e., quaternary, pyrrolic, and pridinic) were observed for the four CPs. Moreover, the pyrrolic and pridinic N species were dominant for $CP_{600-4}$ (Figure 1e), while the two species significantly decreased for the other three CPs (Figure 1f-1h). The differences could be attributed to the relatively lower thermal stability of pyrrolic and pridinic N species, which could be evaporated at higher calcination temperatures (i.e., 600 and 800 °C). C–N configuration also decreased with the increase of calcination temperatures, consistent with the loss of total N in XPS full spectra (Figure S5).

To investigate the defects of the CPs, Raman spectra were collected (Figure 1i–l). It is known that the intensity ratio of peaks at 1360 and 1580 $cm^{-1}$ ($I_D/I_G$) is correlated with the defects of carbon materials. When the temperature increased from 600 to 800 °C, $I_D/I_G$ increased from 0.81 to 0.87, indicating more defect sites were formed in $CP_{600-8}$, which was probably due to the loss of N element at higher temperature.

**Enzyme Mimicking Activities of N-Doped Carbon Nanozymes.** The peroxidase-like activity of the as-prepared CPs were then studied and compared. As shown in Figure S8a, only the system containing TMB, $H_2O_2$ and $CP_{600-6}$ shown obvious color change, demonstrating the intrinsic peroxidase-like activity of $CP_{600-6}$. Besides TMB, the other two substrates (i.e., ABTs and OPD) could also be oxidized in the presence of $H_2O_2$ and $CP_{600-6}$, further confirming the intrinsic peroxidase-like activity of $CP_{600-6}$ (Figure S8b). As expected, the peroxidase-like activity was dependent on the concentrations of $CP_{600-6}$ and $H_2O_2$ (Figure S8c,d).

The peroxidase-like activities of $CP_{600-4}$, $CP_{600-6}$, and $CP_{600-8}$ were compared. It showed that $CP_{600-4}$ exhibited the least activity while $CP_{600-6}$ and $CP_{600-8}$ possessed much higher activity (Figure 2a). This confirmed that thorough carbonization of the MP was needed to obtain highly active peroxidase mimics. To study the effect of PEI molecular weight on the peroxidase-like activity, $CP_{10000-6}$ was fabricated and tested. As shown in Figure 2b, $CP_{600-6}$ had a higher activity than $CP_{10000-6}$. Since $CP_{600-6}$ exhibited the best peroxidase-


DOI: 10.1021/acs.analchem.9b04333
Anal. Chem. 2019, 91, 15267−15274

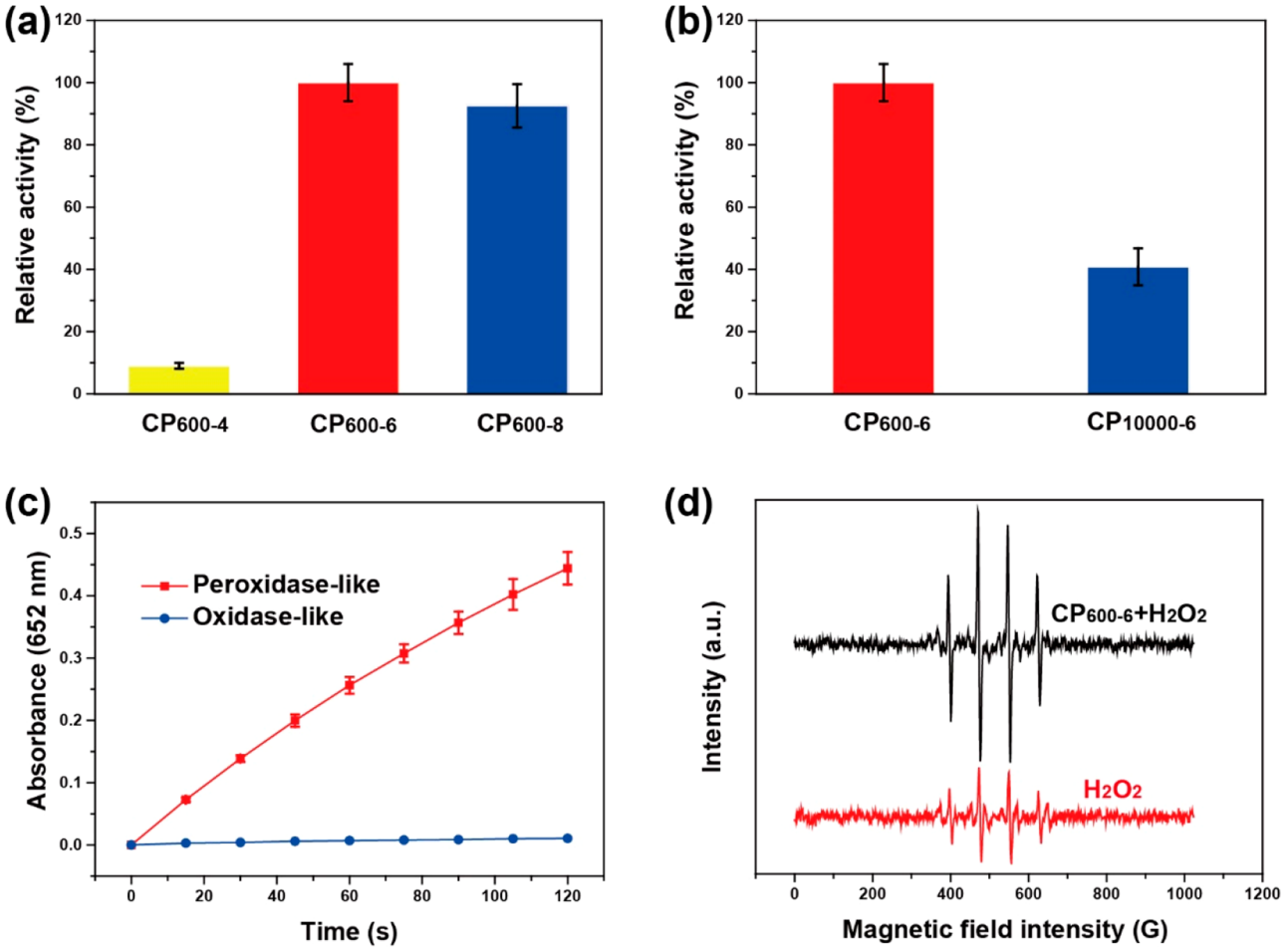


**Figure 2.** Influence of (a) different calcination temperatures and (b) PEI molecular weight on peroxidase-like activity; (c) peroxidase- and oxidase-like activity comparison of $CP_{600-6}$; and (d) EPR spectra of free radicals produced in the catalytic processes.

like activity among the four nanozymes, it was chosen for the following study.

The optimal pH and temperature for the peroxidase-like catalysis of $CP_{600-6}$ were determined. Similar with a natural peroxidase, the activity of $CP_{600-6}$ varied with pH with the maximum at pH 4.0. As for reaction temperature, $CP_{600-6}$ exhibited higher activity with the temperature increase, which was superior to a natural peroxidase (Figure S10).

Other enzyme mimicking activities of $CP_{600-6}$ were also tested. Interestingly, $CP_{600-6}$ exhibited negligible oxidase-, catalase- and SOD-like activities (Figures 2c and S11). This indicated that $CP_{600-6}$ possessed a high and specific peroxidase-like activity.

**Kinetics and Catalytic Mechanism.** Steady-state kinetics assays were performed to obtain the enzymatic kinetic constants including maximum catalytic reaction velocity ($v_{max}$) and affinity toward TMB and $H_2O_2$ ($K_m$) of $CP_{600-6}$ and $CP_{10000-6}$ nanozymes (Figures S12 and S13). Compared with $CP_{10000-6}$, $CP_{600-6}$ had comparable affinity toward TMB but stronger affinity toward $H_2O_2$. Moreover, $CP_{600-6}$ had much larger $v_{max}$ than $CP_{10000-6}$ for both TMB and $H_2O_2$, agreeing with the observed higher peroxidase-like activity of $CP_{600-6}$ (Figure 2b). Interestingly, compared with representative N-doped carbon nanozymes previously reported, $CP_{600-6}$ also exhibited excellent catalytic activity (i.e., higher $v_{max}$), which demonstrated the advantage of our template synthesis method for rationally designing N-doped carbon nanozyme with high peroxidase-like activity (Table S2).

To understand the catalytic mechanism, the catalytic intermediates were studied (Figures 2d and S14). TA and HE were used as the indicators for $^{\bullet}OH$ and $^{\bullet}O_2^-$ radicals, respectively. Only the system containing TA, $H_2O_2$ and $CP_{600-6}$ exhibited high fluorescence intensity, which demonstrated $^{\bullet}OH$ was the catalytic intermediate of the reaction (Figure S14a). On the other hand, no obvious production of $^{\bullet}O_2^-$ was captured in the catalytic process (Figure S14b). To confirm $^{\bullet}OH$ was the only intermediate involved in the peroxidase-like catalysis, the EPR spectra of the reaction system in the presence of DMPO were collected. As shown in Figure 2d, only the EPR signals of $^{\bullet}OH$ were captured, confirming the $^{\bullet}OH$ was the intermediate responsible for the peroxidase-like activity of $CP_{600-6}$.

**Detection of Hydrogen Peroxide, Glucose, and AA.** After the mechanistic study, $CP_{600-6}$ was applied to detect three important bioactive small molecules (i.e., $H_2O_2$, glucose, and AA). Since the peroxidase-like activity of $CP_{600-6}$ was dependent on $H_2O_2$ concentration, $H_2O_2$ could be determined directly. By coupling a glucose oxidase, the concentration of glucose could be further detected (Figure 3a). Then, the detection feasibility of $H_2O_2$ and glucose was confirmed (Figure S15). The linear detection ranges and detection limits were obtained. For $H_2O_2$, a linear detection range between 20 and 200 $\mu$M and a detection limit of 15 $\mu$M were obtained. As


DOI: 10.1021/acs.analchem.9b04333
Anal. Chem. 2019, 91, 15267−15274

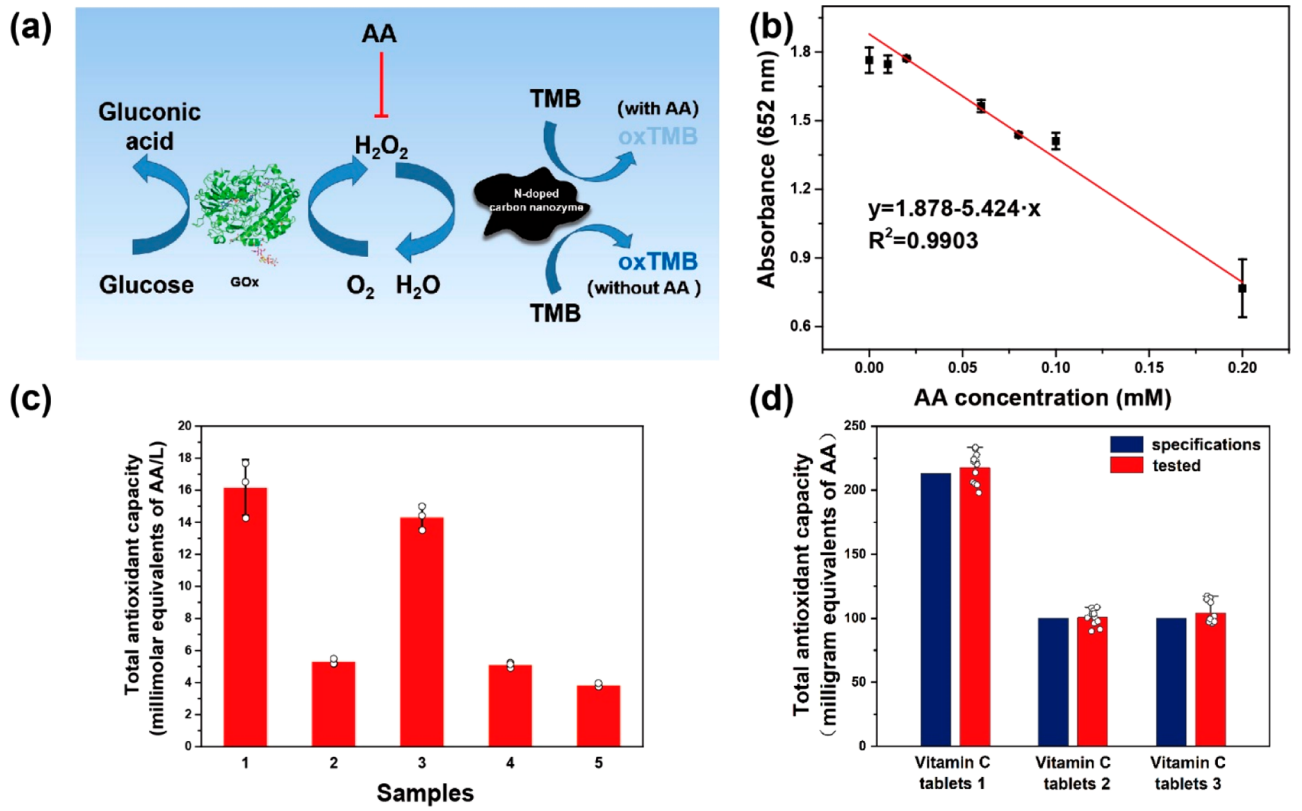


**Figure 3.** (a) Schematic illustration of detecting $H_2O_2$, glucose and AA by using a peroxidase-like N-doped carbon nanozyme (PDB code of GOx: 1CF3). (b) Linear plots of absorbance at 652 nm versus concentrations of AA. (c) TAC of four commercial beverages (marked as 1−4) and fresh orange juice (marked as 5), each error bar shows the standard deviation of three independent measurements; and (d) three vitamin C tablets (the specifications were also shown for comparison). Each error bar shows the standard deviation of 12 independent measurements.

for glucose, a linear detection range between 10 and 100 $\mu$M and a detection limit of 10 $\mu$M were obtained (Figure S16a,b and Table S3). Moreover, several common saccharides (such as fructose, lactose, and sucrose) did not show interference, demonstrating the good selectivity for glucose detection (Figure S16c). As shown in Figure 3a, by competing against the reaction between $H_2O_2$ and TMB, the concentration of AA could be detected. At the optimal pH of 5.0, the absorbance intensity at 652 nm decreased with the concentration of AA increased, demonstrating the detection feasibility of AA (Figure S17). Then, a linear range of 8−80 $\mu$M and a detection limit of 8 $\mu$M were achieved (Figure 3b and Table S3).

**TAC Assays.** TAC is an important indicator to access the quality of antioxidant food and medicine for healthy diet and healthcare. Since the TAC is described as millimolar equivalent of AA/L, we used the above developed detection strategy for AA to evaluate the TAC in several beverages, fresh orange juice, and vitamin C tablets (Figure 3c,d). Samples 1−4 in Figure 3c were four commercial beverages containing vitamin C, and the testing results were consistent with their composition descriptions. Beverages 1 and 3 had higher TAC than 2 and 4. The TAC of the four beverages was higher than fresh orange juice, which may arise from the use of concentrated juice and some antioxidant additives for beverage production. To further demonstrate the practical applications of our TAC assay, the TAC of three kinds of vitamin C tablets were measured. As shown in Figure 3d, the testing results matched the specifications of TAC from the three tablets, suggesting that the tablets have met their qualifications. In order to demonstrate the robustness of the TAC assay, the influence of potential coexistence additives in food and medicine (such as metal ions, amino acids, carbohydrates, GSH, and BSA) on the assay was investigated. As shown in Figure S18, except for cysteine and GSH, other additives did not affect the TAC assay.

## CONCLUSIONS

In conclusion, by utilizing MMT as a template and PEI with high N/C ratio as carbon and nitrogen sources, high N content carbon nanozymes with high and specific peroxidase-like activity were synthesized. The catalytic activity could be facilely modulated by varying the calcination temperatures and PEI molecular weights. The mechanism study revealed that $^{\bullet}OH$ played a key role in the peroxidase-like activity of the carbon nanozymes. Then the assays for $H_2O_2$, glucose, and AA were established, showing satisfactory detection results. Moreover, a TAC assay was developed and successfully used to evaluate the TAC of four commercial beverages, fresh orange juice, and three kinds of vitamin C tablets. Also the detection results met their corresponding composition descriptions or specifications, which demonstrating good prospects for the practical applications in bioactive small molecules detection by using this method. The current work not only developed an effective method to synthesize highly active and specific peroxidase-like nanozymes but also provided a facile way to detect the TAC in food and medical tablets not limited to the above examples.



DOI: 10.1021/acs.analchem.9b04333
*Anal. Chem.* 2019, 91, 15267−15274

## ■ ASSOCIATED CONTENT

### Supporting Information

The Supporting Information is available free of charge on the ACS Publications website at DOI: 10.1021/acs.analchem.9b04333.

Extra figures with associated discussion and tables (PDF)

## ■ AUTHOR INFORMATION


### Corresponding Author

*E-mail: weihui@nju.edu.cn. Web: weilab.nju.edu.cn. Fax: +86-25-83594648. Tel: +86-25-83593272.

### ORCID

Hui Wei: 0000-0003-0870-7142


### Author Contributions

The manuscript was written through contributions of all authors.

### Notes

The authors declare no competing financial interest.

## ■ ACKNOWLEDGMENTS

This work was supported by National Natural Science Foundation of China (21874067 and 21722503), 973 Program (2015CB659400), PAPD Program, Shuangchuang Program of Jiangsu Province, Open Funds of the State Key Laboratory of Analytical Chemistry for Life Science (SKLACLS1704), Open Funds of the State Key Laboratory of Coordination Chemistry (SKLCC1819), Open Funds of Key Laboratory of Analytical Chemistry for Biology and Medicine (Wuhan University), Ministry of Education (ACBM2019001), and Fundamental Research Funds for the Central Universities (021314380145).

## ■ REFERENCES


(1) Gao, L.; Zhuang, J.; Nie, L.; Zhang, J.; Zhang, Y.; Gu, N.; Wang, T.; Feng, J.; Yang, D.; Perrett, S.; Yan, X. *Nat. Nanotechnol.* **2007**, *2*, 577−583.

(2) Huang, Y.; Ren, J.; Qu, X. *Chem. Rev.* **2019**, *119*, 4357−4412.

(3) Jiang, D.; Ni, D.; Rosenkrans, Z. T.; Huang, P.; Yan, X.; Cai, W. *Chem. Soc. Rev.* **2019**, *48*, 3683−3704.

(4) Kotov, N. A. *Science* **2010**, *330*, 188−189.

(5) Ragg, R.; Tahir, M. N.; Tremel, W. *Eur. J. Inorg. Chem.* **2016**, *2016*, 1906−1915.

(6) Tonga, G. Y.; Jeong, Y.; Duncan, B.; Mizuhara, T.; Mout, R.; Das, R.; Kim, S. T.; Yeh, Y.-C.; Yan, B.; Hou, S. *Nat. Chem.* **2015**, *7*, 597−603.

(7) Walther, R.; Winther, A. K.; Fruergaard, A. S.; van den Akker, W.; Sørensen, L.; Nielsen, S. M.; Jarlstad Olesen, M. T.; Dai, Y.; Jeppesen, H. S.; Lamagni, P. *Angew. Chem., Int. Ed.* **2019**, *58*, 278−282.

(8) Wei, H.; Wang, E. *Chem. Soc. Rev.* **2013**, *42*, 6060−6093.

(9) Wu, J.; Wang, X.; Wang, Q.; Lou, Z.; Li, S.; Zhu, Y.; Qin, L.; Wei, H. *Chem. Soc. Rev.* **2019**, *48*, 1004−1076.

(10) Zhang, Z.; Zhang, X.; Liu, B.; Liu, J. *J. Am. Chem. Soc.* **2017**, *139*, 5412−5419.

(11) Zhou, Y.; Liu, B.; Yang, R.; Liu, J. *Bioconjugate Chem.* **2017**, *28*, 2903−2909.

(12) Fan, K.; Cao, C.; Pan, Y.; Lu, D.; Yang, D.; Feng, J.; Song, L.; Liang, M.; Yan, X. *Nat. Nanotechnol.* **2012**, *7*, 459−464.

(13) He, W.; Zhou, Y.-T.; Wamer, W. G.; Hu, X.; Wu, X.; Zheng, Z.; Boudreau, M. D.; Yin, J.-J. *Biomaterials* **2013**, *34*, 765−773.

(14) Jin, L.-Y.; Dong, Y.-M.; Wu, X.-M.; Cao, G.-X.; Wang, G.-L. *Anal. Chem.* **2015**, *87*, 10429−10436.

(15) Liu, Y.; Zhou, M.; Cao, W.; Wang, X.; Wang, Q.; Li, S.; Wei, H. *Anal. Chem.* **2019**, *91*, 8170−8175.

(16) Manea, F.; Houillon, F. B.; Pasquato, L.; Scrimin, P. *Angew. Chem., Int. Ed.* **2004**, *43*, 6165−6169.

(17) Natalio, F.; André, R.; Hartog, A. F.; Stoll, B.; Jochum, K. P.; Wever, R.; Tremel, W. *Nat. Nanotechnol.* **2012**, *7*, 530−535.

(18) Soh, M.; Kang, D. W.; Jeong, H. G.; Kim, D.; Kim, D. Y.; Yang, W.; Song, C.; Baik, S.; Choi, I. Y.; Ki, S. K. *Angew. Chem., Int. Ed.* **2017**, *56*, 11399−11403.

(19) Song, Y.; Qu, K.; Zhao, C.; Ren, J.; Qu, X. *Adv. Mater.* **2010**, *22*, 2206−2210.

(20) Sun, H.; Zhou, Y.; Ren, J.; Qu, X. *Angew. Chem., Int. Ed.* **2018**, *57*, 9224−9237.

(21) Tarnuzzer, R. W.; Colon, J.; Patil, S.; Seal, S. *Nano Lett.* **2005**, *5*, 2573−2577.

(22) Wang, X.; Gao, X. J.; Qin, L.; Wang, C.; Song, L.; Zhou, Y.-N.; Zhu, G.; Cao, W.; Lin, S.; Zhou, L. *Nat. Commun.* **2019**, *10*, 704.

(23) Zhang, W.; Hu, S.; Yin, J.-J.; He, W.; Lu, W.; Ma, M.; Gu, N.; Zhang, Y. *J. Am. Chem. Soc.* **2016**, *138*, 5860−5865.

(24) Duan, D.; Fan, K.; Zhang, D.; Tan, S.; Liang, M.; Liu, Y.; Zhang, J.; Zhang, P.; Liu, W.; Qiu, X. *Biosens. Bioelectron.* **2015**, *74*, 134−141.

(25) Guo, Y.; Deng, L.; Li, J.; Guo, S.; Wang, E.; Dong, S. *ACS Nano* **2011**, *5*, 1282−1290.

(26) Wei, H.; Wang, E. *Anal. Chem.* **2008**, *80*, 2250−2254.

(27) Cheng, H.; Wang, X.; Wei, H. *Anal. Chem.* **2015**, *87*, 8889−8895.

(28) Deng, H.-H.; Luo, B.-Y.; He, S.-B.; Chen, R.-T.; Lin, Z.; Peng, H.-P.; Xia, X.-H.; Chen, W. *Anal. Chem.* **2019**, *91*, 4039−4046.

(29) Gao, Z.; Liu, G. G.; Ye, H.; Rauschendorfer, R.; Tang, D.; Xia, X. *Anal. Chem.* **2017**, *89*, 3622−3629.

(30) Wang, X.; Qin, L.; Zhou, M.; Lou, Z.; Wei, H. *Anal. Chem.* **2018**, *90*, 11696−11702.

(31) Wang, Y.-M.; Liu, J.-W.; Adkins, G. B.; Shen, W.; Trinh, M. P.; Duan, L.-Y.; Jiang, J.-H.; Zhong, W. *Anal. Chem.* **2017**, *89*, 12327−12333.

(32) Zhang, S.; Zhang, D.; Zhang, X.; Shang, D.; Xue, Z.; Shan, D.; Lu, X. *Anal. Chem.* **2017**, *89*, 3538−3544.

(33) Jiao, L.; Xu, W.; Yan, H.; Wu, Y.; Liu, C.; Du, D.; Lin, Y.; Zhu, C. *Anal. Chem.* **2019**, *91*, 11994−11999.

(34) Loynachan, C. N.; Soleimany, A. P.; Dudani, J. S.; Lin, Y.; Najer, A.; Bekdemir, A.; Chen, Q.; Bhatia, S. N.; Stevens, M. M. *Nat. Nanotechnol.* **2019**, *14*, 883−890.

(35) Gao, Z.; Ye, H.; Tang, D.; Tao, J.; Habibi, S.; Minerick, A.; Tang, D.; Xia, X. *Nano Lett.* **2017**, *17*, 5572−5579.

(36) Qin, L.; Wang, X.; Liu, Y.; Wei, H. *Anal. Chem.* **2018**, *90*, 9983−9989.

(37) Wu, Y.-S.; Huang, F.-F.; Lin, Y.-W. *ACS Appl. Mater. Interfaces* **2013**, *5*, 1503−1509.

(38) Huang, L.; Chen, J.; Gan, L.; Wang, J.; Dong, S. *Sci. Adv.* **2019**, *5*, eaav5490.

(39) Fan, K.; Xi, J.; Fan, L.; Wang, P.; Zhu, C.; Tang, Y.; Xu, X.; Liang, M.; Jiang, B.; Yan, X. *Nat. Commun.* **2018**, *9*, 1440.

(40) Hu, Y.; Gao, X. J.; Zhu, Y.; Muhammad, F.; Tan, S.; Cao, W.; Lin, S.; Jin, Z.; Gao, X.; Wei, H. *Chem. Mater.* **2018**, *30*, 6431−6439.

(41) Lin, L.; Song, X.; Chen, Y.; Rong, M.; Zhao, T.; Wang, Y.; Jiang, Y.; Chen, X. *Anal. Chim. Acta* **2015**, *869*, 89−95.

(42) Lin, S.; Zhang, Y.; Cao, W.; Wang, X.; Qin, L.; Zhou, M.; Wei, H. *Dalton Trans.* **2019**, *48*, 1993−1999.

(43) Kim, M. S.; Cho, S.; Joo, S. H.; Lee, J.; Kwak, S. K.; Kim, M. I.; Lee, J. *ACS Nano* **2019**, *13*, 4312−4321.

(44) Yao, H. B.; Tan, Z. H.; Fang, H. Y.; Yu, S. H. *Angew. Chem., Int. Ed.* **2010**, *49*, 10127−10131.

(45) Geng, D.; Yang, S.; Zhang, Y.; Yang, J.; Liu, J.; Li, R.; Sham, T.-K.; Sun, X.; Ye, S.; Knights, S. *Appl. Surf. Sci.* **2011**, *257*, 9193−9198.

(46) Sheng, Z.-H.; Shao, L.; Chen, J.-J.; Bao, W.-J.; Wang, F.-B.; Xia, X.-H. *ACS Nano* **2011**, *5*, 4350−4358.

(47) Ding, W.; Wei, Z.; Chen, S.; Qi, X.; Yang, T.; Hu, J.; Wang, D.; Wan, L. J.; Alvi, S. F.; Li, L. *Angew. Chem., Int. Ed.* **2013**, *52*, 11755−11759.




DOI: 10.1021/acs.analchem.9b04333
*Anal. Chem.* 2019, 91, 15267−15274

(48) Gao, F.; Qu, J.; Geng, C.; Shao, G.; Wu, M. *J. Mater. Chem. A* **2016**, *4*, 7445−7452.
(49) Niu, Q.; Gao, K.; Tang, Q.; Wang, L.; Han, L.; Fang, H.; Zhang, Y.; Wang, S.; Wang, L. *Carbon* **2017**, *123*, 290−298.
(50) Xia, Y.; Mokaya, R.; Walker, G. S.; Zhu, Y. *Adv. Energy Mater.* **2011**, *1*, 678−683.



DOI: 10.1021/acs.analchem.9b04333
*Anal. Chem.* 2019, 91, 15267−15274